sustainability

MDPI

Article

Innovative Use of UHPC and Topology Optimization in Permeable Interlocking Pavers: Advancing Sustainable Pavement Solutions

Fernanda Gadler [1,*], José Augusto Ferreira Sales de Mesquita [2], Francisco Helio Alencar Oliveira [3], Liedi Legi Bariani Bernucci [1], Rafael Giuliano Pileggi [2], Emilio Carlos Nelli Silva [4] and Diego Silva Prado [4]

[1] Department of Transportation Engineering, Polytechnic School of the University of São Paulo, Avenue Professor Luciano Gualberto, No. 380, Butantã, São Paulo 05508-010, SP, Brazil; liedi@usp.br
[2] Department of Civil Construction Engineering, Polytechnic School of the University of São Paulo, Avenue Professor Luciano Gualberto, No. 380, Butantã, São Paulo 05508-010, SP, Brazil; jose.mesquita@lme.pcc.usp.br (J.A.F.S.d.M.); rafael.pileggi@lme.pcc.usp.br (R.G.P.)
[3] Department of Naval Architecture and Ocean Engineering, Polytechnic School of the University of São Paulo, Avenue Professor Luciano Gualberto, No. 380, Butantã, São Paulo 05508-010, SP, Brazil; f.helio@usp.br
[4] Department of Mechatronics and Mechanical Systems Engineering, Polytechnic School of the University of São Paulo, Avenue Professor Luciano Gualberto, No. 380, Butantã, São Paulo 05508-010, SP, Brazil; ecnsilva@usp.br (E.C.N.S.); disprado@usp.br (D.S.P.)
* Correspondence: fernandagadler@usp.br; Tel.: +55-41992778600

Abstract

The rapid expansion of urban areas has increased the prevalence of impermeable surfaces, intensifying flooding risks by disrupting natural water infiltration. Permeable pavements have emerged as a sustainable alternative, capable of reducing stormwater runoff, improving surface friction, and mitigating urban heat island effects. Nevertheless, their broader implementation is often hindered by issues such as clogging and limited mechanical strength resulting from high porosity. This study examines the design of interlocking permeable blocks utilizing ultra-high-performance concrete (UHPC) to strike a balance between enhanced drainage capacity and high structural performance. A topology optimization (TO) strategy was applied to numerically model the ideal block geometry, incorporating 105 drainage channels with a diameter of 6 mm—chosen to ensure manufacturability and structural integrity. The UHPC formulation was developed using particle packing optimization with ordinary Portland cement (OPC), silica fume, and limestone filler to reduce binder content while achieving superior strength and workability, guided by rheological assessments. Experimental tests revealed that the perforated UHPC blocks reached compressive strengths of 87.8 MPa at 7 days and 101.0 MPa at 28 days, whereas the solid UHPC blocks achieved compressive strengths of 125.8 MPa and 146.2 MPa, respectively. In contrast, commercial permeable concrete blocks reached only 28.9 MPa at 28 days. Despite a reduction of approximately 30.9% in strength due to perforations, the UHPC-105holes blocks still far exceed the 41 MPa threshold required for certain structural applications. These results highlight the mechanical superiority of the UHPC blocks and confirm their viability for structural use even with enhanced permeability features. The present research emphasizes mechanical and structural performance, while future work will address hydraulic conductivity and anticlogging behavior. Overall, the findings support the use of topology-optimized UHPC permeable blocks as a resilient solution for sustainable urban drainage systems, combining durability, strength, and environmental performance.

check for updates

Academic Editor: Cara Poor

Received: 31 March 2025
Revised: 16 June 2025
Accepted: 23 June 2025
Published: 1 July 2025

Citation: Gadler, F.; Mesquita, J.A.F.S.d.; Oliveira, F.H.A.; Bernucci, L.L.B.; Pileggi, R.G.; Silva, E.C.N.; Prado, D.S. Innovative Use of UHPC and Topology Optimization in Permeable Interlocking Pavers: Advancing Sustainable Pavement Solutions. *Sustainability* **2025**, *17*, 6039. https://doi.org/10.3390/su17136039

Copyright: © 2025 by the authors. Licensee MDPI, Basel, Switzerland. This article is an open access article distributed under the terms and conditions of the Creative Commons Attribution (CC BY) license (https://creativecommons.org/licenses/by/4.0/).

Keywords: permeable pavements; urban flooding; ultra-high-performance concrete (UHPC); hydraulic conductivity; topology optimization (TO); sustainable infrastructure

1. Introduction

Rapid urban growth has led to significant changes in land use and occupation, bringing a complex set of economic, social, and environmental impacts. This exponential urbanization leads to the construction of new buildings, pavements, and sidewalks, which increase the impermeable areas of cities, thereby intensifying flooding by disrupting natural water cycles [1]. In this context, pavement infrastructure plays a crucial role in the sustainability of urban systems [2]. Specifically, permeable pavements contribute to enhancing this ecosystem, significantly benefiting the urban environment by reducing stormwater runoff volume, increasing skid resistance on pavement surfaces, and minimizing traffic noise and the urban heat island effect [3].

Although permeable pavements offer promising benefits to both built and natural environments, challenges that threaten their long-term effectiveness—especially concerning maintenance and clogging of pores—remain key barriers to their widespread application [3]. Additionally, the inverse relationship between porosity and concrete strength limits the use of permeable paving blocks to light traffic roads or pedestrian pathways, as conventional permeable pavements rely on high porosity to achieve sufficient permeability and, consequently, are low-strength systems [4].

While the hydraulic capacity, drainage potential, and anticlogging performance of the proposed interlocking permeable blocks are recognized as essential for the effectiveness of permeable pavements, these aspects are not the primary focus of the present study and will be comprehensively addressed in a future publication dedicated to evaluating hydraulic performance. Instead, this article concentrates on the innovative application of ultra-high-performance concrete (UHPC) combined with topology optimization, emphasizing the structural design and mechanical performance. The research explores how UHPC's exceptional strength enables the creation of optimized geometries that balance mechanical resistance with permeability, ensuring structural integrity without compromising durability.

2. Research Scope and Significance

This study focuses on the innovative design of interlocking permeable blocks using ultra-high-performance concrete (UHPC) combined with topology optimization (TO) to balance mechanical strength and hydraulic conductivity. The primary emphasis of this article is on the structural performance of the optimized block, ensuring that the mechanical requirements are met for practical application. While the drainage potential and hydraulic performance of the proposed design are recognized as essential aspects, these will be comprehensively addressed in a separate publication dedicated to hydraulic evaluation. The experimental phase in this study validates the feasibility of producing durable, structurally sound, anticlogging permeable blocks suitable for sustainable urban infrastructure.

3. Literature Review

As cities expand, urban areas become increasingly susceptible to flooding due to impermeable surfaces that limit rainwater absorption. Flood events, whether minor or severe, are occurring more frequently and have a substantial impact on individuals, businesses, and infrastructure. In the United Kingdom alone, flood-related damages amount to billions annually [4].

Permeable pavements are widely recognized for their hydrological benefits, reducing surface runoff and mitigating flood peaks. Studies indicate runoff reductions between 50% and 100% compared to conventional pavements [5], and flood peak reductions up to 90%, even with low-drainage subbases. In newly urbanized areas, these systems can lower development costs by reducing the need for additional drainage infrastructure, with stormwater volume reductions reaching 70–90%, similar to natural landscapes like fields or forests [6].

Permeable paving blocks, forming the surface layer of these systems, offer dual functionality: adequate structural performance and environmental benefits. They function as drainage elements while contributing to air quality improvement [7].

Despite these advantages, certain limitations hinder the broader use of permeable pavements. Chief among them is the mechanical behavior of porous concrete, which is closely linked to its high porosity [8–10]. Because compressive strength and porosity are inversely related, these blocks are often restricted to low-traffic applications like sidewalks and bike paths.

Another limitation is the decline in infiltration capacity over time due to clogging by sediments and dust. National and international standards set requirements for the infiltration rate, which must remain above 10^{-5} m/s, as per ICPI guidelines [11]. Although pressurized water jets can restore permeability, optimizing the design to reduce maintenance frequency also supports sustainability goals.

A key factor in clogging is the tortuosity of the pore network, which disrupts flow and promotes obstruction. Redesigning pore structures to reduce tortuosity is a promising strategy. Some authors also advocate for higher compressive strength to expand permeable pavements to heavier load applications [4]. However, high porosity often compromises strength, limiting conventional systems to light loads.

Engineering design plays a critical role in sustainable solutions. Within ecological engineering, ecodesign integrates environmental considerations from the early planning stages [12]. Topology optimization (TO), widely used in fields like aerospace and bioengineering [13], offers a method for achieving optimal material distribution based on criteria such as stiffness or weight [14].

In this manuscript, TO is applied to balance mechanical strength and hydraulic conductivity in the block design. Although hydraulic testing will be presented separately, TO proved fundamental in reconciling structural integrity and permeability in a single solution. The algorithm iteratively determines material distribution, allowing efficient optimization. Applied to civil engineering, TO contributes to sustainability by reducing material use and greenhouse gas emissions [15].

UHPC (ultra-high-performance concrete) offers high strength and low porosity, enhancing durability and performance in adverse conditions [16–18]. It is particularly suited for pavements exposed to loads, moisture, and deicing agents. Its dense microstructure also supports longer service life and reduced maintenance.

Recent research focuses on designing low-tortuosity pore networks to improve drainage and reduce maintenance. Advanced modeling techniques can establish quantitative links between pore characteristics and pavement performance, enabling more effective and resilient permeable blocks [5].

In summary, this article proposes a resilient engineering solution for urban drainage using interlocking permeable blocks. The design incorporates topology optimization and UHPC to achieve structural and environmental performance. This approach supports cities in addressing climate change impacts and improving urban infrastructure resilience.

4. Materials and Methods

This section presents the materials and methods adopted in the present study. Initially, the numerical modeling techniques and proposed validation procedures are detailed, focusing on the design and optimization of the seep-sink block geometry. Subsequently, the experimental validation is described, based on performance tests carried out with the permeable blocks produced using an ultra-high-performance concrete (UHPC) mixture.

4.1. Seep-Sink-Block Design—Numerical Optimization

The numerical optimization techniques employed in this study provided an initial approach to optimizing the block design, focusing on introducing openings that would provide sufficient drainage capacity while maintaining mechanical strength. This strategy aimed to address two key and often conflicting requirements in the development of permeable pavers: enhancing hydraulic conductivity and ensuring structural integrity. By integrating these numerical findings, the subsequent experimental phase was directed toward validating the feasibility of the optimized design under real-world mechanical and functional conditions.

Following this concept, the block was designed with permeable ducts as an integral part of its structure rather than just an incidental characteristic of the concrete composition. The diameter of the flow channels was defined as 6 mm, based on technical and safety criteria for urban pavement applications. This dimension aims to prevent risks to pedestrian safety, particularly for women wearing high-heeled shoes, whose base of support typically measures less than 10 mm. According to a technical study conducted by Belgard Architectural Products Group [19], heels with widths of up to 9 mm were tested on pavements with 10 mm joints, highlighting the need to limit openings to prevent accidents such as tripping or heel entrapment. Therefore, adopting openings of 6 mm or less represents an appropriate and safe solution for urban environments, effectively minimizing the risk of footwear entrapment on permeable surfaces. Additionally, in the numerical simulation, a manufacturing criterion was applied to incorporate the maximum possible number of ducts into the block while ensuring moldability and structural integrity. This approach resulted in a configuration with 105 holes, balancing hydraulic performance with structural safety. The main objective of this stage is to obtain a topologically optimized design for a pavement block that maximizes permeability per square meter while maintaining mechanical strength according to ABNT 9781 standards for light traffic, light vehicles, and commercial line vehicles. The key requirements are based on the premise of minimum permeability of 10^{-3} m/s (ABNT NBR 16416:2015 [20]). Using linear elasticity theory for a prism under axial load, the axial stress $\sigma(x)$ is defined by Equation (1).

$$\sigma(x) = \frac{P(x)}{A} \tag{1}$$

where P(x) is the axial force and A is the cross-sectional area. The resulting elastic deformation follows Hooke's Law: $\sigma(x) = E \cdot \varepsilon(x)$, where E is Young's modulus and $\varepsilon(x) = du/dx$ (displacement gradient) [21].

For the failure analysis, the safety factor (F_{safety}) was calculated based on the Mohr–Coulomb criterion (Figure 1), which was chosen over the von Mises criterion due to its more accurate representation of concrete's asymmetric behavior in tension and compression. This criterion is defined by Equation (2).

$$F_{safety} = \left[\frac{\sigma_1}{S_{UT}} + \frac{\sigma_3}{S_{UC}} \right]^{-1} \tag{2}$$

where, σ_1 = maximum principal stress, σ_3 = minimum principal stress, σ_1 and σ_3 from FEA, S_{UT} = tensile strength, S_{UC} = compressive strength, S_{UT} and S_{UC} from Table 1.

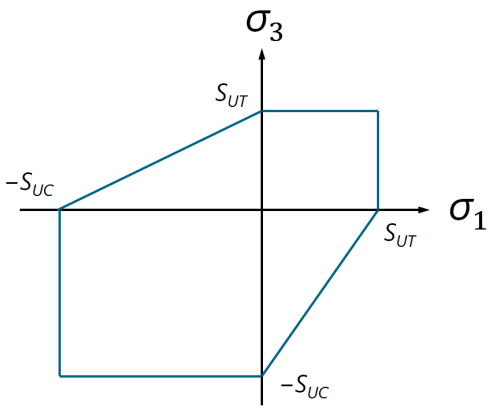


Figure 1. Mohr-Coulomb criteria.

Table 1. Properties using FEA analyses.

Properties	Units	Steel Plate	COMMERCIAL	UHPC
Solid Density	kg/m^3	7850	2300	2470
Poisson's ratio		0.30	0.18	0.15
Young's Modulus	MPa	210×10^3	25×10^3	56×10^3
Tensile Strength	MPa	800	6.1	16
Compressive Strength	MPa	960	35	130

To fulfill the specified requirements, the following procedural steps were implemented:

1. Geometric modeling: A three-dimensional model of a standard block (200 × 100 × 60 mm) was initially designed using ANSYS SpaceClaim (Version R2 2024), adhering to standard block geometry. A quarter-symmetry approach was adopted to reduce computational effort.
2. Material assignment: the geometry was imported into ANSYS Workbench (Version R2 2024), where linear elastic, isotropic, uncracked, and homogeneous material properties were assigned based on the parameters listed in Table 1.
3. Finite element discretization: The model was discretized using the finite element method (FEM) with a structured hexahedral mesh (Figure 2). A high-order 20-node SOLID186 element formulation was employed to ensure numerical accuracy and convergence in the mechanical response analysis.
4. Boundary conditions and loading configuration:

The numerical model constrained the block's degree of freedom (DOF) along the Z-axis, while permitting unrestricted translational movement in the X and Y directions. The specimen was positioned between two high-hardness steel plates (60 Rockwell C) with an 85 mm diameter and 20 mm thickness.

A compressive load was applied to achieve the minimum specified 28-day compressive strength (f_{pk}) of 35 MPa, as prescribed by ABNT NBR 9781:2013 [22]. The loading protocol followed a quasistatic analysis to maintain consistency with the normative loading rate requirement of 550 kPa/s, to simulate standardized testing conditions.

ANSYS Workbench provides an integrated CAD/CAE environment, enabling streamlined mechanical behavior analysis and facilitating future design optimization through parametric geometry modifications. The parameters used as input for the numerical study were defined based on the values proposed in Mesquita's (2024) Master's dissertation [23].

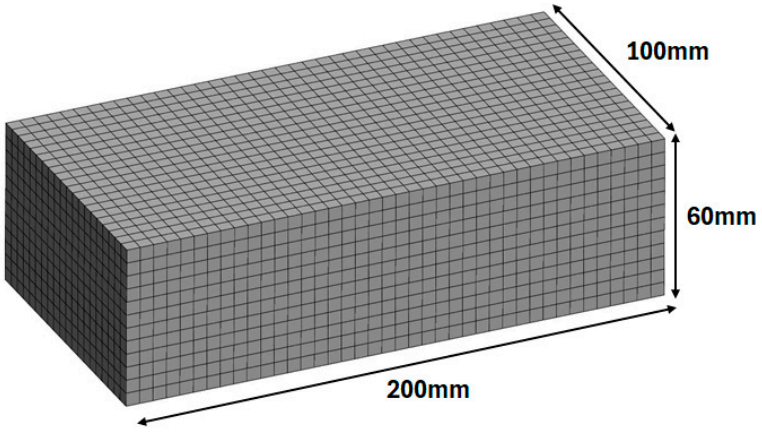


Figure 2. Mesh details of standard block (FEM).

Adding fluid flow channels increases stress levels, which depend on the material properties, load conditions, and brick design. Therefore, it is necessary to use a material with higher compression strength. Manufacturing constraints were considered for the next steps, and the maximum number of fluid flow channels (each with a 6 mm diameter) was added. Static FEA will then be conducted to verify the maximum stress under load, and based on these results, the minimum required strength of the replacement material will be determined.

For modifying the standard geometry, a minimum linear distance equal to the channel diameter will be assumed to ensure moldability and prevent shrinkage and void issues. Under these constraints, the following configuration was obtained as shown in Figure 3. The FEM mesh details are as follows: element type, Hexa SOLID186, 2nd order; 84,378 elements and 372,687 nodes, as illustrated in Figure 4.

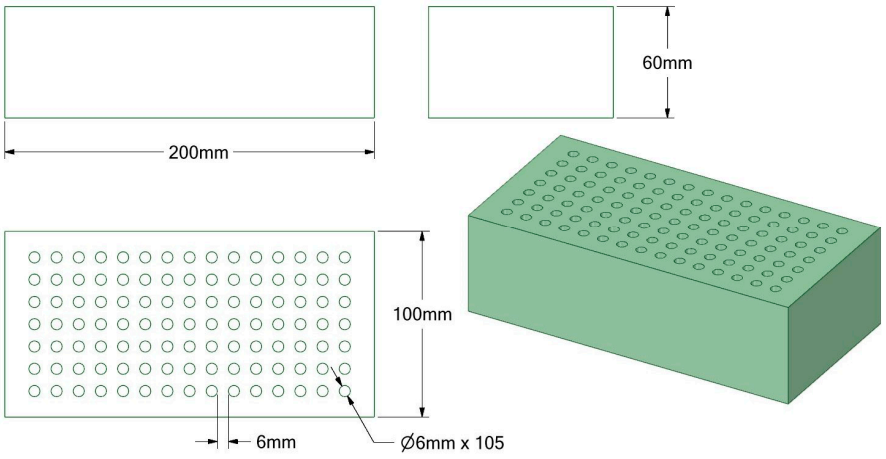


Figure 3. CAD geometry of optimized block.

Thus, the numerical modeling based on topological optimization criteria was essential for establishing the design premises of the permeable block, guiding its geometric configuration, the sizing of the drainage channels, and the selection of mechanical properties suitable for structural performance. This initial step enabled the conceptual adjustment of the block, effectively balancing hydraulic requirements with structural integrity in accordance with applicable technical standards. The adopted strategy aimed to anticipate, through simulation, the operational limits and material strength demands imposed by the designed openings, providing a rational foundation for prototype development. With the optimized model validated numerically, the research advanced to the experimental phase,

focused on verifying the mechanical performance of the blocks through laboratory testing, thereby confirming the practical feasibility of the proposed solution.

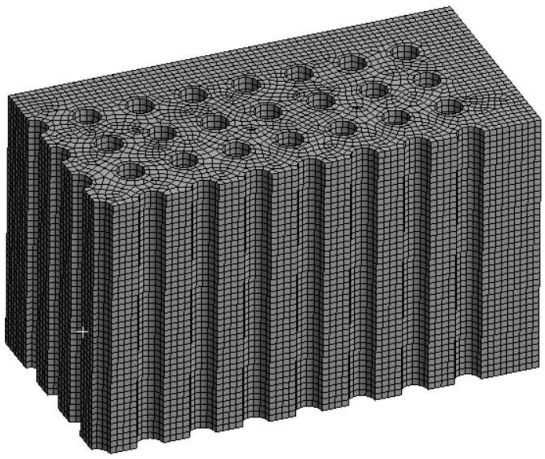


Figure 4. Mesh details of optimized block.

4.2. Experimental Validation

4.2.1. Materials and Mix Design

This study employed ordinary Portland cement (OPC; type CP-V—Holcim), microcement (MC), and silica fume (SF; Elkem 971U, São Paulo, SP, Brazil) to improve both packing efficiency and pozzolanic reactivity. To enhance sustainability and reduce binder demand, the mix design incorporated two grades of limestone filler (LF1 and LF5) as partial replacements for cementitious materials. Additionally, two quartz sands with distinct particle size distributions (Sand-1 and Sand-5) were selected to optimize granular packing. The combination of fine and coarse sands contributed to the formation of a dense granular skeleton, minimizing porosity and further improving the material's performance.

The particle size distribution of fine materials (<10^6 μm) was measured using laser diffraction (Helos, Sympatec, São Paulo, SP, Brazil; 0.1–355 μm range). Sand gradation was assessed using dynamic image analysis (QicPic, Sympatec; 100–4000 μm range). Real density was determined by helium pycnometry (Multipycnometer, Quantachrome, São Paulo, SP, Brazil), and specific surface area (SSA) by BET analysis (Belsorp Max, Bel Japan, São Paulo, SP, Brazil) [24,25]. Figure 5 shows the particle size curves. Table 2 summarizes the SSA, real density, and D10–D90 values of each material.

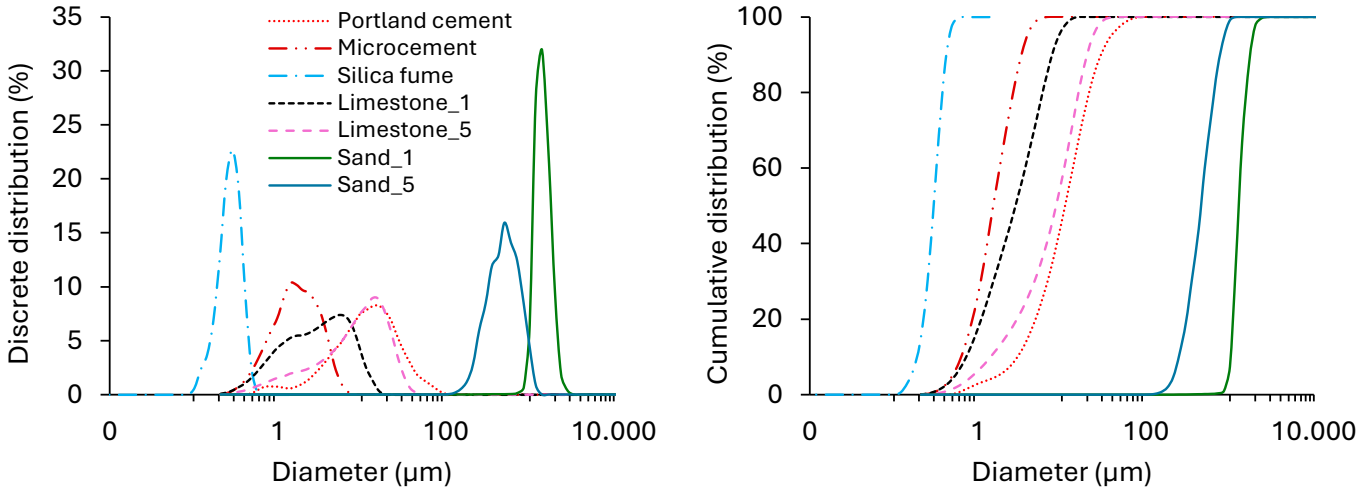


Figure 5. Particle size distribution of raw materials.

Table 2. Physical properties of the used materials.

Raw Material	D10 (μm)	D50 (μm)	D90 (μm)	SSA (g/cm^3)	Density (g/cm^3)
OPC	2.81	9.46	26.76	1.26	3.09
MC	0.59	1.41	2.81	4.03	2.95
SF	0.196	0.301	0.435	23.7	2.19
LF1	0.70	2.37	6.69	3.43	2.78
LF5	1.41	7.95	18.92	1.03	2.78
Sand_1	1000	1180	1700	0.02	2.67
Sand_5	212	425	710	0.04	2.66

OPC and LF5 had similar D50 values, though OPC showed a narrower distribution. Microcement exhibited a smaller size range, indicating better packing potential. Silica fume, with D50 below 0.3 μm and high SSA, enhances packing and nucleation during hydration [26–28].

The chemical composition of the fine materials was determined using X-ray fluorescence (XRF) with an Axios Advanced spectrometer (Panalytical, São Paulo, SP, Brazil) [24]. Table 3 presents the oxide compositions. The cements comply with NBR 16697, which limits SO_3 to <4.5%, loss on ignition (LOI) to <6.5%, MgO to <6.5%, and insoluble residue to <3.5%.

Table 3. Chemical characteristics of raw materials, obtained by XRF.

Chemical Species	OPC (%)	MC (%)	SF (%)	LF (%)
SiO_2	19.2	30.7	97.3	4.52
Al_2O_3	4.94	9.79	0.30	0.11
Fe_2O_3	2.97	0.86	0.10	<0.10
CaO	60.8	42.2	0.40	48.4
MgO	0.67	5.66	0.20	5.89
SO_3	4.47	5.92	0.20	<0.10
Na_2O	0.15	0.45	0.20	<0.10
K_2O	0.70	0.60	0.30	<0.10
TiO_2	0.25	0.66	<0.10	<0.10
P_2O_5	0.27	<0.10	<0.10	<0.10
MnO	0.09	0.23	<0.10	<0.10
SrO	0.27	0.07	<0.10	<0.10
L.O.I	3.87	3.07	0.60	41.0

MC had lower CaO but higher Al_2O_3 and SiO_2 than OPC, indicating a higher C_2S/C_3S ratio and suggesting slower reactivity. Its elevated MgO content reflects a more dolomitic nature. SO_3 exceeded the NBR limit, likely due to higher gypsum addition to control aluminate reactivity.

Silica fume was composed mainly of SiO_2 (>97%), reinforcing its pozzolanic potential [26]. Limestone filler showed low SiO_2 (~4.5%) and higher MgO, confirming its dolomitic origin. Its L.O.I (41%) was slightly below the theoretical value for pure limestone (44%), suggesting minor impurities.

The paste mix design used in this study was developed in a previous work by Mesquita [23], aiming to reduce binder demand while maintaining high mechanical performance and workability. Aggregate proportions were defined using the particle packing model proposed by Westman and Hugill [29], aiming to achieve a dense granular skeleton with minimal porosity. This model promotes the efficient arrangement of particles of varying sizes, improving packing density and reducing the binder requirement.

A single optimized composition was developed following this methodology. The detailed mix design and material consumption are summarized in Table 4. Further information can be found in Mesquita [23].

Table 4. Material consumption for the optimized mix design.

Raw-Materials	Consumption (kg/m^3)
OPC	351
MC	91
SF	44
LF1	409
LF5	162
Sand-1	498
Sand-2	762
Water	153
w/s	0.06
w/b	0.31

The mix design achieved a low water-to-solids (w/s) ratio of 0.06, which contributes to a dense microstructure with reduced capillary porosity [23]. In contrast, the water-to-binder (w/b) ratio of 0.31 ensures a sufficient level of hydration, as it directly influences the extent of binder reaction. While low w/s values are desirable to limit porosity and enhance durability, excessively low w/b ratios may impair hydration and compromise strength development [15]. Therefore, formulations should aim to minimize water-to-solid (w/s) ratios while maintaining a sufficiently high water-to-binder (w/b) ratio to ensure effective hydration kinetics and mechanical performance.

4.2.2. Casting

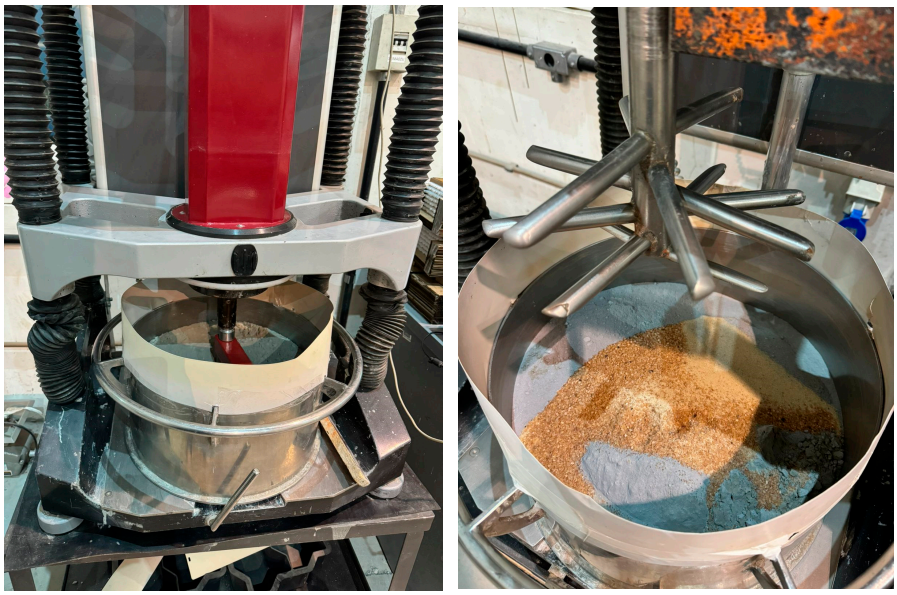
The mixing process was performed using a Pheso rheometer, manufactured by Calmetrix (São Paulo, SP, Brazil) (Figure 6a), to evaluate the rheological behavior during mixing and determine the applicable rheological parameters. The test geometry chosen was of the attritor type, positioned in a planetary system, allowing for efficient and homogeneous mixing of the materials.

Initially, the dry materials (cement, silica fume, limestone filler, and sand) were added to the mixing vessel of the rheometer (Figure 6b). The dry mixing was carried out at a speed of 100 rpm for 180 s, ensuring the homogenization of the components before adding water. After this step, the water was added gradually at a flow rate of 50 g/s, using a funnel equipped with a rubber hose and a control valve.

Once the water was completely added, the mixing continued for 10 min at a speed of 186 rpm, ensuring proper dispersion of the materials and complete hydration of the binders. This process allowed the achievement of proper consistency in the development of UHPC, while maintaining the necessary rheological properties for its application.

The blocks were produced using the molding technique, which is suitable for the type of UHPC mixture. The samples were molded (Figure 7a) in reinforced cardboard molds, laser-cut (200 × 100 × 60mm), designed to meet the shape requirements and ensure the proper positioning of the channels. To prevent water absorption by the cardboard and facilitate demolding, the molds were coated with adhesive tape, which acted as both a release agent and a barrier against water ingress. As defined in the methodology, 6mm plastic tubes were positioned to create the pre-existing channels in the piece. After mixing

the concrete, the specimens were cast (Figure 7b,c) and kept in a dry chamber for 24 h, under controlled conditions of 23 °C and 50% relative humidity. After this period, the blocks were carefully demolded, and the plastic straws used to form the channels were manually removed, ensuring the proper opening of the flow ducts. Given the surface characteristics of UHPC, the removal of the plastic straws was greatly facilitated, leaving no material inside the openings or any residual debris. Subsequently, the specimens were placed in a moist curing chamber at a constant temperature of 23 °C and 100% relative humidity, where they remained for 28 days, completing the curing cycle according to the parameters recommended for concrete mechanical strength testing. Some specimens, however, were removed after 7 days for intermediate testing purposes.



(**a**) (**b**)

Figure 6. Mixing process of UHPC. (**a**) mixing process using a Pheso rheometer; (**b**) dry materials added to the mixing vessel of the rheometer.



(**a**) (**b**) (**c**)

Figure 7. Sample preparation by casting. (**a**) prepared molds before casting; (**b**) UHPC mixture being cast into the molds; (**c**) mold fully filled with self-compacting UHPC mixture.

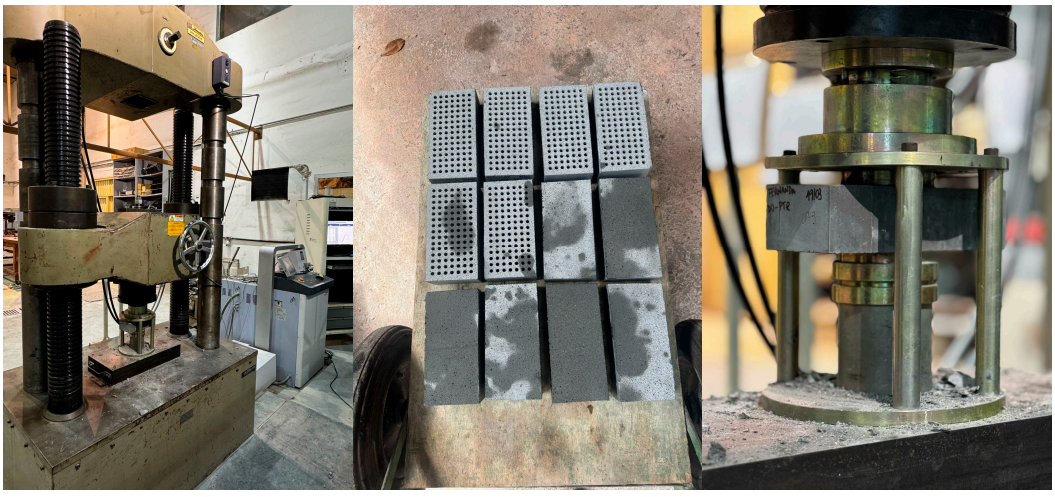
4.2.3. Mechanical Performance

Compressive Strength

A compression test was conducted to determine the minimum compressive strength in accordance with Standard ABNT NBR 9781:2013 and ASTM C109 [30]. According to this norm, the test specimens should conform to Type I, with a rectangular shape and dimensions of 200 × 100 × 60 mm. The shape factor (IF), defined as the ratio between the specimen's length and height, must be less than or equal to 4; in this case, IF = 200/60 = 3.3, which meets the standard's requirement. The application of this type of block is suitable for pedestrian traffic, light vehicles, and commercial vehicles. The minimum compressive strength required by the norm is 35 MPa. For the experimental analysis, a total of 18 specimens were produced: 6 UHPC blocks without any holes (UHPC-0holes), 6 UHPC blocks with 105 holes (UHPC-105holes) based on the proposed geometry, and 6 commercially available permeable concrete blocks commonly used in Brazil (commercial). All specimens were manufactured with identical dimensions to ensure accurate and fair comparison among the different types of blocks and their respective structural configurations. The concrete mixtures were tested for compressive strength at curing ages of 7 and 28 days.

Compressive strength tests were performed using a Shimadzu universal testing machine (capacity: 2000 kN) (Shimadzu, São Paulo, SP, Brazil). Specimens were ground to ensure parallel loading surfaces. The test aimed to assess the influence of binder reduction on the hardened-state performance of UHPC.

Figure 8 presents the testing apparatus, which includes the compression testing machine, the specimens (UHPC-0holes, UHPC-105holes, and commercial), and the complete setup used for the compressive strength evaluation. This visual reference supports the methodological description by illustrating the experimental conditions under which the tests were conducted.



(**a**) (**b**) (**c**)

Figure 8. Compressive test (**a**) testing machine (**b**) specimens (**c**) apparatus and setup.

Dynamic Modulus of Elasticity

The dynamic modulus of elasticity was determined using the Ultrasonic Pulse Velocity (UPV) test, which employed a device operating in pulse-echo mode (Pundit Lab, 200 kHz frequency, Ø 20 mm transducers). To ensure proper contact and minimize signal loss during wave transmission, the transducers were coupled to the surface of the specimens using medical-grade ultrasonic gel. After applying the gel, the transducers were positioned on opposite faces of the specimen, aligned and parallel to each other, ensuring a straight-line propagation of the ultrasonic pulse (Figure 9). The measurement of the wave's time of flight

across the material allowed the calculation of the ultrasonic wave velocity. Based on this data and the physical properties of the concrete (density and Poisson's ratio), the dynamic modulus of elasticity was estimated using linear elasticity equations, in accordance with ABNT NBR 8802:2019 and ASTM C597 standards [31,32].

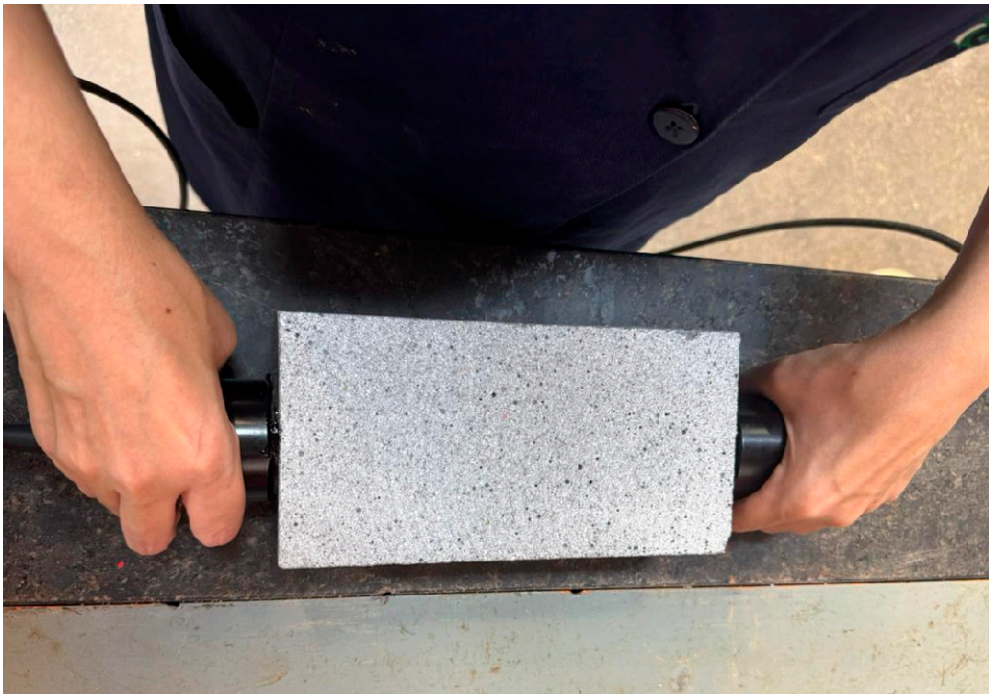


Figure 9. Ultrasonic pulse velocity (UPV) test setup.

5. Results and Discussion

5.1. Seep-Sink-Block Design—Numerical Optimization

Adding fluid flow channels increases stress levels, which depend on the material properties, load conditions, and the block design. Therefore, it is necessary to use a material with higher compressive strength. The manufacturing constraints were considered, and the maximum number of fluid flow channels (each with a 6 mm diameter) was added. Then, a static FEA analysis was performed to verify the maximum stress under load, and based on these results, the minimum required strength of the replacement material was determined.

Furthermore, to adapt the standard geometry, a minimum linear distance equivalent to the channel diameter was maintained to ensure moldability and mitigate potential defects such as shrinkage and void formation. Under these design constraints, Figure 10 demonstrates that incorporating flow channels in UHPC does not compromise structural strength, as the material's inherent resistance exceeds the imposed stress limits. Furthermore, the compressive load specified by ABNT NBR 9781 imposes a minimum material strength requirement of 35 MPa and the incorporation of fluid flow channels increases the induced stress to 41 MPa.

Figure 11 presents the Mohr-Coulomb safety factors for three specimen types: COMMERCIAL without holes, COMMERCIAL with holes, and UHPC with holes. Consequently, the candidate replacement material must exhibit a minimum compressive resistance of 41 MPa. In this context, ultra-high-performance concrete (UHPC) presents a viable solution for optimizing permeable blocks, ensuring structural integrity while maintaining the necessary drainage capacity.

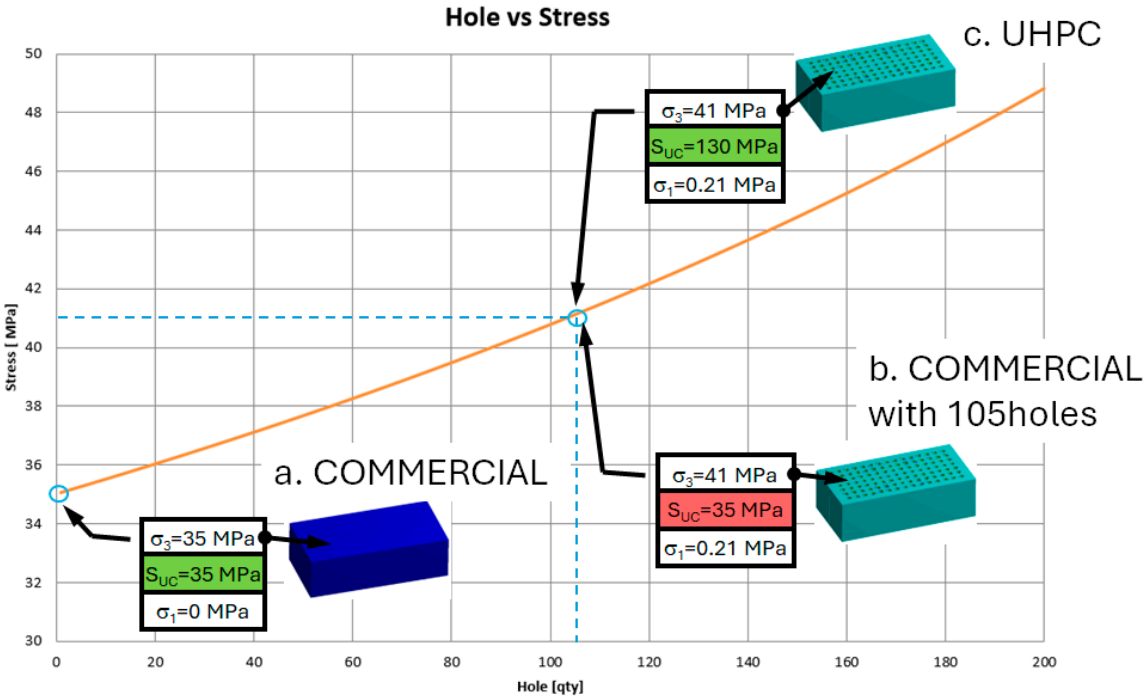


Figure 10. Stress distribution per hole in the optimized block.

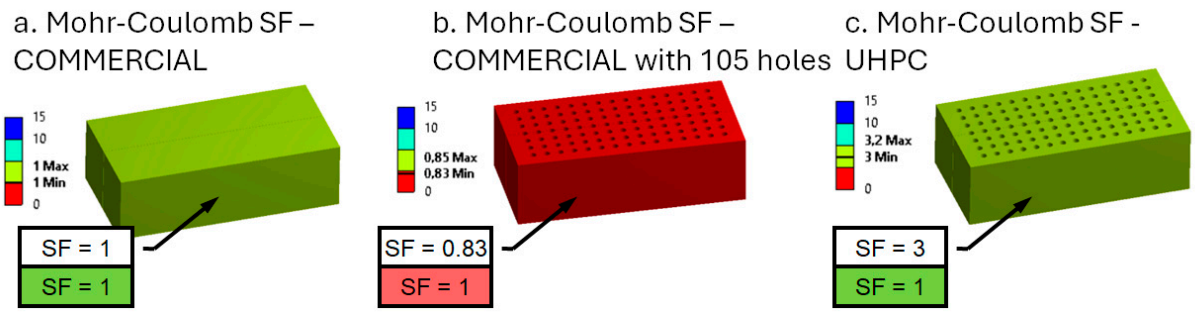


Figure 11. Mohr-Coulomb safety factor.

5.2. Experimental Validation

5.2.1. Mix Design

Aiming to reduce binder consumption and enhance its efficiency, a mixture was developed using a high volume of inert addition, which improved the properties of UHPC, achieving a compressive strength of 120 MPa after 28 days. This approach is complex because a higher proportion of fine materials can influence water demand and alter rheological properties, thereby affecting the hydration process. In response to the changes in the specific surface area (SSA) of the fines and considering the mineralogy of the addition, it was necessary to adjust the water content for the mixture.

It is important to emphasize the significance of considering rheological variables in developing UHPC mixtures with mineral additions, from processing to the material's performance properties. The mechanical strength tests at 28 days were performed to assess the effect of inert addition content in UHPC, resulting in a mixture with a strength of 130 MPa.

5.2.2. Casting

From a molding point of view, casting proved to be quite efficient, and did not create any problems during concreting. The self-compacting characteristic of UHPC facilitated

the procedure, and even with the very dense quantity of pipes, which could cause concrete failures, there were no problems in this regard, as seen in the produced block shown in Figure 12.

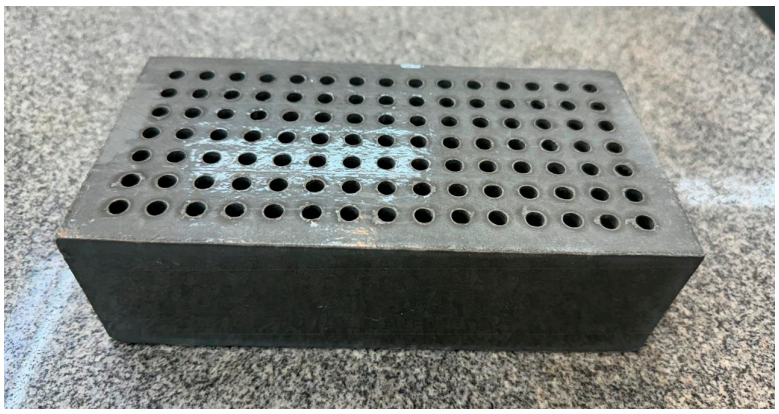


Figure 12. Optimized block.

5.2.3. Mechanical Performance

Compressive Strength

Figure 13 illustrates the compressive strength results for the three block types—UHPC-0holes, UHPC-105holes, and COMMERCIAL.

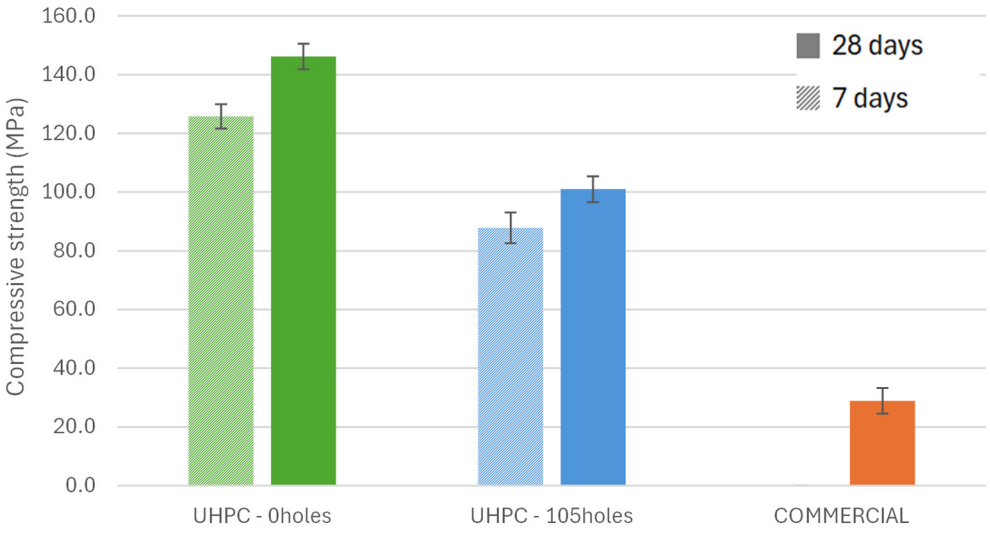


Figure 13. Compressive strength results for the three block types: UHPC-0holes, UHPC-105holes, and COMMERCIAL.

The results of the compressive strength tests, as presented in the table, show significant differences among the three types of blocks. The UHPC-0holes blocks (solid, with no holes) exhibited the highest average compressive strength, reaching 125.8 MPa at 7 days and 146.2 MPa at 28 days, with standard deviations of 4.14 MPa and 4.36 MPa, respectively. The UHPC-105holes blocks, which contain 105 perforations designed to enhance permeability, achieved compressive strengths of 87.8 MPa at 7 days and 101.0 MPa at 28 days, with standard deviations of 5.20 MPa and 4.41 MPa, respectively. This corresponds to a reduction of approximately 30.9% at 28 days compared to the solid UHPC blocks, yet still well above the 41 MPa threshold required for certain structural applications, as confirmed by finite element analysis (FEA). In contrast, the commercial permeable concrete blocks (COMMERCIAL) demonstrated significantly lower performance, with an average of 28.9 MPa at 28 days,

with a standard deviation of 4.36 MPa. Despite their lower performance, these commercial blocks still meet the minimum requirement of 20 MPa defined by ABNT NBR 9781:2013 for low-traffic permeable pavements. These findings underscore the superior mechanical performance of UHPC blocks, particularly the UHPC-0holes, and reveal that even with a high degree of perforation, the UHPC-105holes maintain structural integrity while offering enhanced permeability.

According to the reference studies in the literature, the compressive strength of conventional pervious concrete blocks typically ranges from 1 MPa to 28 MPa, and may reach up to 46 MPa when enhanced with additives such as silica fume, fine aggregates, and superplasticizers [33–35]. More recent research [4] reports compressive strengths between 6 and 32 MPa for pervious concretes with porosities ranging from 12% to 32%, showing an inverse relationship between strength and void content. In contrast, concretes with preformed ducts—similar to those proposed in this manuscript—have achieved strengths ranging from 19 MPa to 59 MPa, significantly surpassing the structural and pavement application thresholds. Within this context, the results presented in this article stand out substantially, particularly the UHPC-based blocks, which demonstrate compressive strengths far superior to conventional benchmarks, even in highly perforated configurations.

Dynamic Modulus of Elasticity

Figure 14 illustrates the dynamic modulus of elasticity results for the three block types, UHPC-0holes, UHPC-105holes, and commercial—measured using the ultrasonic pulse velocity (UPV) method.

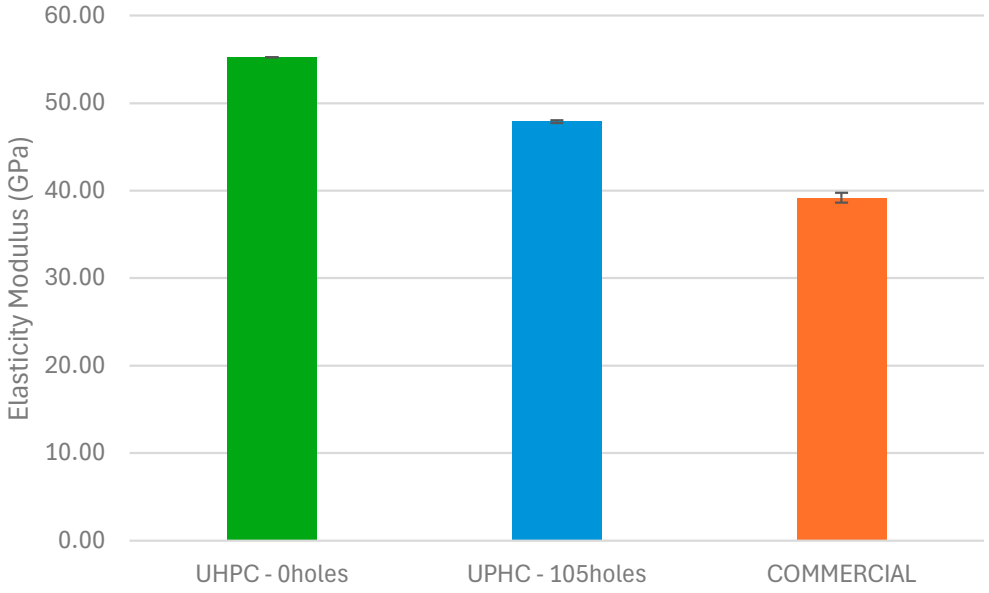


Figure 14. Dynamic modulus of elasticity results for the three block types: UHPC-0holes, UHPC-105holes, and COMMERCIAL.

The results demonstrated that both UHPC blocks, 0holes and 105 holes, exhibited superior stiffness compared to the commercial concrete block. The UHPC-0holes blocks reached an average modulus of 48 GPa, while the UHPC-105holes blocks showed 45 GPa, against 32 GPa for the COMMERCIAL. These values represent an increase of 28.9% to 33.3% over the commercial alternative. The presence of 105 perforations led to only a 6.25% reduction in modulus, confirming the structural efficiency of the duct geometry and its minimal impact on ultrasonic wave propagation. Compared to the literature, some authors [36] reported values ranging from 22 to 24 GPa for porous concretes, while

others [37] observed values between 40.5 and 46.7 GPa in conventional concretes cured up to 56 days. Moreover, the literature [4] emphasized the influence of air content on UPV measurements, noting that even a 6% air content could reduce wave velocity by up to 10%.

6. Conclusions

This paper demonstrates the potential of UHPCs to meet high standards of sustainability and workability in special block geometries with a high density of pipes, without compromising the material's mechanical properties, such as strength and durability. Moreover, the results indicate that the mechanical resistance properties remained unaffected while maintaining the material's high drainage capacity. These results encourage the continuation of studies focusing on the durability and other performance characteristics of UHPC, enabling significant advancements in the use of this concrete type in sustainable infrastructures, such as permeable pavements.

The numerical modeling techniques employed in this research were essential for defining the key parameters and the optimal design of the permeable interlocking block. Through topology optimization and finite element analyses, it was possible to establish a geometry that balances mechanical strength and hydraulic performance. These numerical approaches guided the experimental phase, which subsequently validated the predicted mechanical behavior, confirming the reliability and accuracy of the simulations. The successful correlation between numerical predictions and experimental results reinforces numerical modeling as a powerful and indispensable tool for fostering innovation in the development of advanced permeable pavement systems and sustainable urban infrastructure solutions.

The seep-sink blocks with integrated linear ducts, as developed in this research, offer a highly efficient solution for stormwater management in urban environments. Their optimized design enhances surface permeability and accelerates water infiltration through engineered duct pathways, significantly reducing runoff and the risk of localized flooding. Unlike conventional permeable pavers, the UHPC composition provides superior mechanical strength and durability, making these blocks suitable for high-load traffic areas while maintaining their hydraulic function over time. Additionally, the linear ducts serve as microdrainage channels, promoting consistent flow and reducing the likelihood of clogging, thereby contributing to the long-term performance and resilience of urban drainage systems.

The manufacturing process can be adjusted and optimized for large-scale commercial production, making it feasible for broader application in the construction industry. Future studies could explore process modifications, material optimization, and cost-effectiveness to enhance scalability while maintaining the desired mechanical and functional properties. This presents a promising research direction to bridge the gap between experimental development and industrial implementation.

Additionally, the surface of the blocks should be further studied through the development of microtextures to enhance safety and prevent accidents. Future research could focus on optimizing surface patterns to improve slip resistance while maintaining the material's durability and drainage capacity.

Future studies should specifically address the hydrological performance of the proposed interlocking permeable blocks, including detailed evaluations of hydraulic conductivity and anticlogging behavior under long-term service conditions. As a continuation of this research, it is recommended to investigate the influence of the geometric arrangement of the drainage holes through advanced numerical simulations and the development of new internal configurations. These efforts aim further to optimize both the hydraulic performance and resistance to clogging, thereby enhancing the overall efficiency and durability of permeable blocks for sustainable urban infrastructure applications.

Based on the results demonstrating the high drainage capacity of the block, new hole configurations can be explored to meet design specifications for temporary water storage in urban pavements. This could help reduce peak flooding events and contribute to the development of large-scale stormwater management systems, enhancing urban resilience to heavy rainfall.

Author Contributions: Conceptualization, F.G. and L.L.B.B.; methodology, F.G. and J.A.F.S.d.M. and F.H.A.O.; software, F.G. and J.A.F.S.d.M. and F.H.A.O.; validation, F.G., L.L.B.B., J.A.F.S.d.M. and R.G.P.; formal analysis, F.G.; investigation, F.G.; resources, F.G., J.A.F.S.d.M. and F.H.A.O.; data curation, F.G.; writing—original draft preparation, F.G.; writing—review and editing, F.G., J.A.F.S.d.M., F.H.A.O., L.L.B.B., R.G.P., E.C.N.S. and D.S.P.; visualization, F.G., J.A.F.S.d.M., F.H.A.O., L.L.B.B., R.G.P., E.C.N.S. and D.S.P.; supervision, L.L.B.B., R.G.P. and E.C.N.S.; project administration, F.G. and L.L.B.B.; funding acquisition, F.G., L.L.B.B., E.C.N.S. and D.S.P. All authors have read and agreed to the published version of the manuscript.

Funding: This research was funded by Fundação de Apoio à Universidade de São Paulo—Grant No. 10087/494; by the Productivity Research Fellowship from CNPq—CNPq Grant No. 304508/2023-3; and by the financial support of FAPESP under Grant No. 2023/10333-9.

Institutional Review Board Statement: Not applicable.

Informed Consent Statement: Not applicable.

Data Availability Statement: Data is contained within the article. The original contributions presented in this study are included in the article. Further inquiries can be directed to the corresponding author.

Conflicts of Interest: The authors declare no conflict of interest.

Abbreviations

The following abbreviations are used in this manuscript:

UHPC	Ultra-High-Performance Concrete
FEA	Finite Element Analysis
OPC	Ordinary Cement Portland
ABNT	Associação Brasileira de Normas Técnicas
NBR	Norma Brasileira
TO	Topology Optimization
CAD	Computer-Aided Design
CAE	Computer-Aided Engineering
SF	Silica Fume
LF1	Limestone Filler 1
LF5	Limestone Filler 5
DfM	Design for Manufacturing
MC	Microcement
SSA	Specific Surface Area
LOI	Loss On Ignition
ASTM	American Society for Testing and Materials
ICPI	Interlocking Concrete Pavement Institute
DOF	Degree Of Freedom
GHG	Greenhouse Gas

References

1. Barua, P.; Saha, A.K. Climate Change Impact on Migration Situation in Coastal Delta Belt of Bangladesh: A Qualitative Explorative Study. *J. Clim. Change* **2024**, *10*, 51–68. [CrossRef]
2. Federal Highway Administration (FHWA). *Highway Statistics Series*; U.S. Department of Transportation: Washington, DC, USA, 2011. Available online: http://www.fhwa.dot.gov (accessed on 12 August 2024).
3. Xie, N.; Akin, M.; Shi, X. Permeable Concrete Pavements: A Review of Environmental Benefits and Durability. *J. Clean. Prod.* **2019**, *210*, 1605–1621. [CrossRef]
4. Kia, A.; Wong, H.S.; Cheeseman, C.R. High-Strength Clogging Resistant Permeable Pavement. *Int. J. Pavement Eng.* **2021**, *22*, 271–282. [CrossRef]
5. Kia, A. Permeable Concrete Pavements for a Climate Change Resilient Built Environment. *Adapt. Built Environ. Clim. Change* **2023**, *15*, 297–326. [CrossRef]
6. Foster, J.; Lowe, A.; Winkelman, S. *The Value of Green Infrastructure for Urban Climate Adaptation*; Center for Clean Air Policy: Washington, DC, USA, 2011.
7. Jamshidi, A.; Kurumisawa, K.; White, G.; Nishizawa, T.; Igarashi, T.; Nawa, T.; Mao, J. State-of-the-Art of Interlocking Concrete Block Pavement Technology in Japan as a Post-Modern Pavement. *Constr. Build. Mater.* **2019**, *200*, 713–755. [CrossRef]
8. Haselbach, L.M.; Batezini, R.; Dutra, V.; Schwetz, P.; Filho, L.C.P.S.; Curvo, F.; Balbo, J.T. Nondestructive Method for Estimating Porosity of In-Situ Pervious Concrete. *J. Test. Eval.* **2016**, *45*, 1726–1735. [CrossRef]
9. Kevern, J.; Schaefer, V.R.; Wang, K. Mixture Proportion Development and Performance Evaluation of Pervious Concrete for Overlay Applications. *ACI Mater. J.* **2011**, *108*, 439–448.
10. Schaefer, V.R.; Wang, K.; Muhannad, T.S.; Kevern, J.T. *Mix Design Development for Pervious Concrete in Cold Climates*; Final Report, Iowa State University: Ames, IA, USA, 2006.
11. Interlocking Concrete Pavement Institute (ICPI). *Permeable Interlocking Concrete Pavements: Selection, Design, Construction and Maintenance*, 3rd ed.; Interlocking Concrete Pavement Institute (ICPI): Burlington, NJ, USA, 2006.
12. Pioch, S.; Relini, G.; Souche, J.C.; Stive, M.J.F.; De Monbrison, D.; Nassif, S.; Simard, F.; Allemand, D.; Saussol, P.; Spieler, R.; et al. Enhancing eco-engineering of coastal infrastructure with eco-design: Moving from mitigation to integration. *Ecol. Eng.* **2018**, *120*, 574–584. [CrossRef]
13. Zhu, J.-H.; Zhang, W.-H.; Xia, L. Topology optimization in aircraft and aerospace structures design. *Arch. Comput. Methods Eng.* **2016**, *23*, 595–622. [CrossRef]
14. Silva, C.O. *Sistema de Piso com Peças de Concreto [Livro Eletrônico]: Pavimento Intertravado-Manual de Desempenho*, 1st ed.; Associação Brasileira de Cimento Portland (ABCP); Associação Brasileira da Indústria de Blocos de Concreto-BlocoBrasil: São Paulo, Brazil, 2022.
15. Oliveira, F.H.; Picelli, R.; Silva, E.C.; Barari, A.; Romano, R.C.; Pileggi, R.G.; Tsuzuki, M.S. Topology Optimization in 3D Concrete Printing to Reduce Greenhouse Gas Emissions. *IFAC-PapersOnLine* **2024**, *58*, 634–639. [CrossRef]
16. Azmee, N.M.; Shafiq, N. Ultra-High Performance Concrete: From Fundamental to Applications. *Case Stud. Constr. Mater.* **2018**, *9*, e00197. [CrossRef]
17. Gu, C.; Ye, G.; Sun, W. Ultrahigh Performance Concrete-Properties, Applications and Perspectives. *Sci. China Technol. Sci.* **2015**, *58*, 587–599. [CrossRef]
18. Bahmani, H.; Mostofinejad, D. Microstructure of Ultra-High-Performance Concrete (UHPC)–A Review Study. *J. Build. Eng.* **2022**, *50*, 104118. [CrossRef]
19. Belgard Architectural Products Group. High Heel Shoes & Belgard® Permeable Pavers. 2018. Available online: https://www.belgardcommercial.com/wp-content/uploads/2023/10/Belgard-Technical-Note-High-Heel-Shoes-and-Belgard-Permeable-Pavers.pdf (accessed on 21 April 2025).
20. *ABNT NBR 16416:2015*; Pervious Concrete Pavement—Requirements and Procedures. Associação Brasileira de Normas Técnicas: Rio de Janeiro, Brazil, 2015.
21. Timoshenko, S.; Goodier, J.N. *Theory of Elasticity*, 2nd ed.; McGraw-Hill: New York, NY, USA, 1951.
22. *ABNT NBR 9781:2013*; Concrete Paving Units—Specification and Test Methods. Associação Brasileira de Normas Técnicas: Rio de Janeiro, Brazil, 2013.
23. Mesquita, J.A.F.S. Ultra-high Performance Concrete (UHPC) eco-efficient: Strategies to minimize mixing energy and binder consumption. Master's Dissertation, Polytechnic School of the University of São Paulo, Department of Civil Construction Engineering, São Paulo, Brazil, 2024; 168p.
24. Maciel, M.H.; Soares, G.S.; de Oliveira Romano, R.C.; Cincotto, M.A. Monitoring of Portland cement chemical reaction and quantification of the hydrated products by XRD and TG in function of the stoppage hydration technique. *J. Therm. Anal. Calorim.* **2019**, *136*, 1269–1284. [CrossRef]
25. Mantellato, S.; Palacios, M.; Flatt, R.J. Relating early hydration, specific surface and flow loss of cement pastes. *Mater. Struct.* **2019**, *52*, 5. [CrossRef]

26. Sealey, B. Silica fume for high performance concrete. In Proceedings of the Uluslararası 10. Beton Kongresi, 3rd Session, 46th Term Proceedings, Istanbul, Turkey, 2–4 May 2019.
27. Romano, R.C.O.; Schreurs, H.; John, V.M.; Pileggi, R.G. Influência da técnica de dispersão nas propriedades de sílica ativa. *Cerâmica* **2008**, *54*, 456–461. [CrossRef]
28. Zain, M.; Safiuddin, M.; Mahmud, H. Development of high performance concrete using silica fume at relatively high water–binder ratios. *Cem. Concr. Res.* **2000**, *30*, 1501–1505. [CrossRef]
29. Westman, A.E.R.; Hugill, H.R. The Packing of Particles. *J. Am. Ceram. Soc.* **1930**, *13*, 767–779. [CrossRef]
30. *ASTM C109*; Standard Test Method for Compressive Strength of Hydraulic Cement Mortars (Using 2-in. or [50-mm] Cube Specimens). ASTM International: West Conshohocken, PA, USA, 2020.
31. *ABNT NBR 8802:2019*; Hardened Concrete—Determination of Ultrasonic Wave Transmission Velocity. Associação Brasileira de Normas Técnicas: Rio de Janeiro, Brazil, 2019.
32. *ASTM C597*; Standard Test Method for Ultrasonic Pulse Velocity Through Concrete. ASTM International: West Conshohocken, PA, USA, 2023.
33. Ibrahim, A.; Mahmood, A.H.; Hamid, R.; Taha, M.R. Experimental and analytical study on properties of pervious concrete for pavement applications. *Constr. Build. Mater.* **2014**, *50*, 524–529. [CrossRef]
34. Lian, C.; Zhuge, Y. Optimum mix design of enhanced permeable concrete–An experimental investigation. *Constr. Build. Mater.* **2010**, *24*, 2664–2671. [CrossRef]
35. Tennis, P.D.; Leming, M.L.; Akers, D.J. *Pervious Concrete Pavements*; PCA Serial No. 2828; Portland Cement Association (PCA): Washington, DC, USA, 2004; Available online: https://www.cement.org (accessed on 21 August 2024).
36. Silva, M.F.; Gomes, A.C.; Rodrigues, J.P. Recycled materials in paving blocks: Sustainable solutions for the construction industry. *Constr. Build. Mater.* **2020**, *247*, 118539. [CrossRef]
37. de Camargo, M.V. Evaluation of the Permeability and Elastic Modulus of Concretes with Different Fine-Aggregate Contents. Master's Thesis, Universidade Estadual de Maringá, Maringá, Brazil, 2018. Available online: https://pcv.uem.br/documentos/dissertacao-de-mestrado/dissertacao_marcos-vinicio-de-camargo_entrega-1.pdf (accessed on 18 April 2025).

Disclaimer/Publisher's Note: The statements, opinions and data contained in all publications are solely those of the individual author(s) and contributor(s) and not of MDPI and/or the editor(s). MDPI and/or the editor(s) disclaim responsibility for any injury to people or property resulting from any ideas, methods, instructions or products referred to in the content.